ANALYSIS OF PRESTRESSED CONCRETE CONTAINMENT VESSEL (PCCV) UNDER SEVERE ACCIDENT LOADING

SANG HOON NOH*, IL HWAN MOON[1], JONG BO LEE and JONG HAK KIM
Korea Hydro & Nuclear Power Co., Ltd. (KHNP), 25-1 Jang-Dong, Yuseong-Gu, Daejeon, Korea
[1]Korea Power Engineering Company Inc., Yong-in, GyeongGi-do, Korea
*Corresponding author. E-mail : shnoh@khnp.co.kr

Received July 5, 2007
Accepted for Publication November 16, 2007

This paper describes the nonlinear analyses of a 1:4 scale model of a prestressed concrete containment vessel (PCCV) using an axisymmetric model and a three-dimensional model. These two models are refined by comparison of the analysis results and with testing results. This paper is especially focused on the analysis of behavior under pressure and the temperature effects revealed using an axisymmetric model.

The temperature-dependent degradation properties of concrete and steel are considered. Both geometric and material nonlinearities, including thermal effects, are also addressed in the analyses. The Menetrey and Willam (1995) concrete constitutive model with non-associated flow potential is adopted for this study. This study includes the results of the predicted thermal and mechanical behaviors of the PCCV subject to high temperature loading and internal pressure at the same time.

To find the effect of high temperature accident conditions on the ultimate capacity of the liner plate, reinforcement, prestressing tendon and concrete, two kinds of analyses are performed: one for pressure only and the other for pressure with temperature. The results from the test on pressurization, analysis for pressure only, and analyses considering pressure with temperatures are compared with one another. The analysis results show that the temperature directly affects the behavior of the liner plate, but has little impact on the ultimate pressure capacity of the PCCV.

KEYWORDS : Containmnet Vessel, Pressure Loading, FE Analysis, Loading History

1. INTRODUCTION

Predicting the response of a prestressed concrete containment vessel (PCCV) is very important for the safety of a nuclear power plant. In addition, there are growing concerns about the performance of containment vessels under severe accident pressures. Hence, a more realistic evaluation of the PCCV behavior due to postulated overpressure is necessary to maintain containment integrity.

In this paper, a prediction of the response of the Sandia National Laboratories 1:4 scale PCCV [1] model is made through various types of numerical modeling, taking in account the appropriate non-linearity for each material. For the nonlinear finite element analysis, the PCCV is idealized as an axisymmetric model and a three-dimensional global model. In order to simulate the actual behavior of the PCCV, both numerical models are refined by comparison of the results of the two analyses and with the existing research results. Furthermore, more recently developed material models for concrete are introduced to the finite elements models. One is Menetrey-Willam's concrete failure criterion, which is used for the axisymmetric global model, and the other is a modified Drucker-Prager's model, which is used for the three-dimensional global model.

This paper is mainly focused on finding the effects of high temperature accident conditions on the ultimate pressure capacity of the PCCV. For this study, the analyses are performed for two kinds of loading cases, using an axisymmetric model : one is a saturated steam condition, which is a loading condition within the range of temperatures that does not change material properties; the other is the Station Blackout (SBO) loading condition, which is a representative severe accident scenario, including pressure with temperature.

2. MATERIAL MODEL

2.1 General

To simulate the PCCV, the actual (tested) properties of concrete, reinforcing steel, post-tensioning tendon, liner plate, and soil are used in the analysis. The properties for these materials are from test data provided by Sandia National Laboratories and used in the construction of the 1:4-scale PCCV at Sandia. The strength reductions induced by an increase of temperature are appropriately introduced to account for material degradation, since high accident temperatures are introduced with accident pressure to the PCCV model.

2.2 Concrete

2.2.1 Constitutive Model

The concrete is characterized by a materially nonlinear deformation behavior. The material non-linearity is assumed to occur due to cracking of concrete under tension and plasticity of concrete under compression. However, the material non-linearity due to the latter has relatively less influence than that due to the former on the failure mode of the containment structure under internal pressure.

The Menetrey-Willam's failure model and modified Drucker-Prager's model with a non-associated plastic flow that is known to be suitable to represent the tensile concrete cracking of the finite element model are introduced in the numerical analysis [2]. The yield surface and flow potential parameters for the elasto-plastic material yield surface in the Menetrey-Willam's failure model with non-associated plastic flow and strain hardening are defined by the model parameters r-factor, the friction angle β, and the dilation angle ψ. The elliptic function $r(\theta,e)$ controls the shape of the yield surface in the deviatoric plane and angle β is the angle between the yield surface and the pressure stress axis in the meridian plane [3].

In the modified Drucker-Prager failure model, the yield surface and flow potential parameters for elasto-plastic material are defined by setting of the model parameters such as the K-factor, the friction angle β, and the dilation angle ψ. [4]. Tension stiffening effects are represented in two aspects, as follows. The first is to modify the stiffness of reinforcing bars embedded in concrete, and the second is to modify the stiffness of the concrete [5].

2.2.2 Material Properties

The following mechanical concrete properties from the uniaxial strength test data of the trial mix concrete are used in the analysis of the 1:4 scale PCCV model for mechanical (internal pressure load only) and thermal-mechanical (pressure + temperature) loading.

Table 1. Concrete Material Property

Property	Basemat	Shell & Dome
Elastic Modulus	27,950 MPa	26,970 MPa
Compressive Strength	39.16 MPa	47.30 MPa
Tensile Strength	3.37 MPa	3.45 MPa
Poisson's Ratio	0.18	0.18

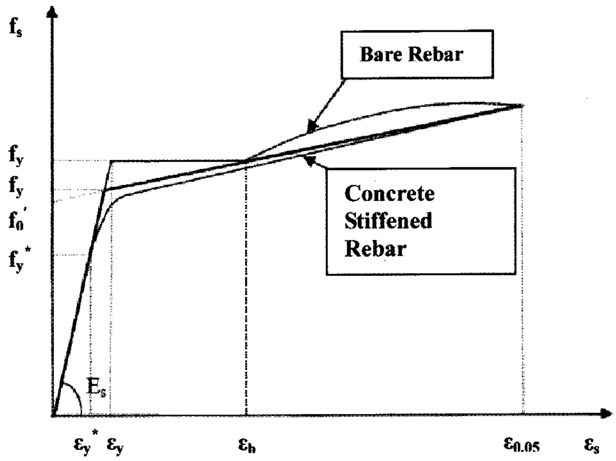

Fig. 1. Stress-Strain Relationship of Rebar

2.3 Reinforcement Steel (Rebar)

2.3.1 Constitutive Model

Rebar materials are generally incompressible when they deform plastically and their yielding is independent of the pressure stress. The von Mises failure criterion is used for this steel material. Hsu [6] noted that the stress-strain curves for bare steel bar and for steel bar embedded in concrete are quite different, as shown in Figure 1. Therefore, the stress-strain relationship of rebar embedded in concrete has been used in reinforced concrete structure to simulate the realistic behavior of the rebar in concrete.

The stress-strain curve of the rebar for the numerical analysis is idealized by a bilinear curve with a slope of E_s before yielding and a slope of E_p after yielding, as illustrated in Figure 1. The equations of the two lines are expressed at the stress level designated by f_y', at which the two straight lines intersect, as shown in equations (1) and (2). The plastic modulus E_p'after yielding can be taken as a small fraction of the elastic modulus E_s.

$$f_s = E_s \varepsilon_s \quad \text{for } f_s \le f_y' \tag{1}$$

$$f_s = f_o' + E_p' \varepsilon_s \quad \text{for } f_s \rangle f_y' \tag{2}$$

where f_o' is the vertical intercept of the post-yield straight line.

The intersection stress level f_y' and the plastic modulus E_p' depend mainly on the level of the apparent yield stress f_y^* illustrated in Figure 1. The apparent yield stess ratio f_y^*/f_y is sensitive to the reinforcement ratio ρ and the solution can be expressed as an average equation (3), where f_{cr} is the cracking strength of concrete. The values of f_y' and E_p' in the stress-strain relatinship used in the numerical analysis are calculated via equations (4) and (5) using the apparent yield stress f_y^* and the strain-hardening modulus of the bare bar E_p from the actual material properties.

$$\frac{f_y^*}{f_y} = 1 - \frac{4}{\rho}\left(\frac{f_{cr}}{f_y}\right)^{1.5} \quad (3)$$

$$\frac{f_y'}{f_y} = 0.43 + 0.5\frac{f_y^*}{f_y} \quad (4)$$

$$\frac{E_p'}{E_p} = 3.3 - 2.5\frac{f_y^*}{f_y} \quad (5)$$

2.3.2 Material Property

The test results provided in the Appendix of References [1] are used in the numerical modeling of the rebar material properties. Table 2 presents the modulus of elasticity for each type and each size of the reinforcement steel.

Table 2. Typical Rebar Material Properties (unit: MPa)

	D16 (SD390)	D19 (SD390)	D22 (SD390)
Elastic Modulus	1.83X10^5	1.84 X10^5	1.91 X10^5
Poisson's ratio	0.3	0.3	0.3
Yield Stress	457.5	473.1	459.0
Tensile Stress	616.5	658.3	680.8
Extension (%)	22.1	21.1	18.7

2.4 Prestressing Tendon

2.4.1 Material Model

The stress-strain curve of a bare prestressing tendon comprised of two straight lines joined by a knee curve, as shown in Figure 2, is used in the numerical analysis. The first part of the curve is a straight-line up to $0.7f_{pu}$, and the second part is expressed by the Ramberg-Osgood equation (6) that meets the first part at the stress level of $0.7f_{pu}$.

$$f_p = \frac{E_{ps}'\varepsilon_p}{\left[1 + \left(\frac{E_{ps}'\varepsilon_p}{f_{pu}}\right)^4\right]^{1/4}} \quad (6)$$

where f_{pu}, f_p, f_{ps}' and ε_p are the ultimate strength of the tendon, the strength in the tendon, the tangential modulus Ramberg-Osgood curve at zero load and the sum of strain in the tendon, respectively [6].

ABAQUS, the finite element program, has no function to incorporate the unbonded tendon. The prestressing tendons are modeled as rebar subelements in concrete using the embedded approach available in ABAQUS. The numerical modeling of tendons as rebar sub-elements implies that the tendons are assumed bonded to the concrete and slippage of the tendon in the tendon sheath is not considered in the numerical analysis.

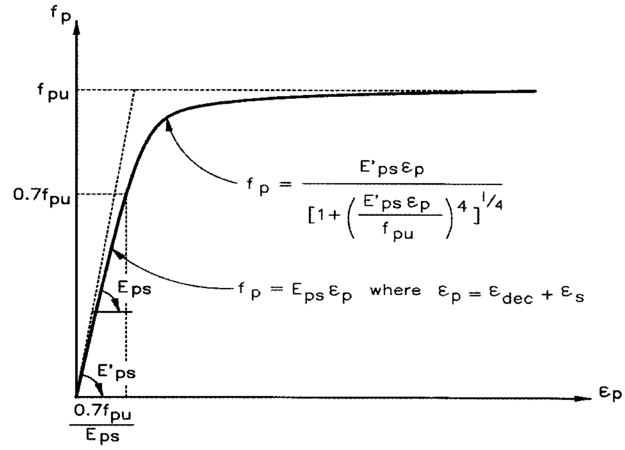

Fig. 2. Stress-Strain Relationship of Prestressing Tendon

2.4.2 Material Property

The material properties shown in Table 3 are used for the tendon modeling.

Table 3. Tendon Material Properties

Property	Values
Elastic Modulus	218,700 MPa
Yield Strength	375.6 MPa
Poisson's Ratio	0.3
Ultimate Tensile Strength	499.2 MPa

2.5 Steel Liner Plate

2.5.1 Constitutive Model

The stress-strain behavior of the liner plate steel is modeled by using an elasto-plastic model. The von Mises failure surface with kinematic hardening is used to represent the nonlinear behavior of the material.

2.5.2 Material Property

The material properties of the liner plate used in the numerical analysis are shown in Table 4.

Table 4. Steel Liner Material Properties

Property	Values
Elastic Modulus	191,000 MPa
Elastic Limit Stress	1,339 MPa
Yield Strength	1691 MPa
Poisson's Ratio	0.3
Ultimate Strength	1,912 MPa
Extension	4.5%

2.6 Changes of Material Properties Due to Temperature

The material properties of concrete, rebar, tendon, and liner steel include the tendency to lose resistant capability due to various chemical and mechanical phenomena as temperature increases. The results of previous empirical studies on the effects of temperature increase on material properties are shown in Fig. 3 [7, 8].

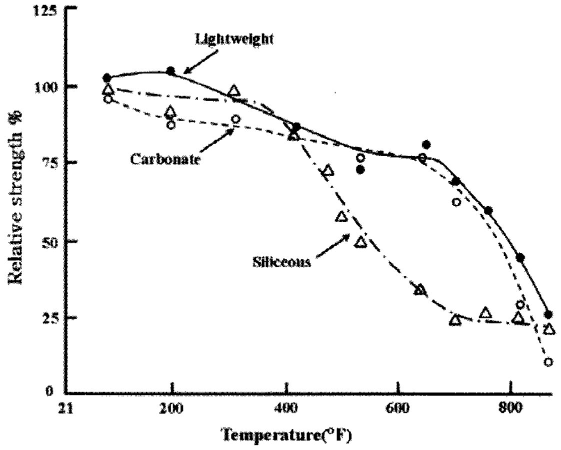

(a) Compression Strength Ratio [7]

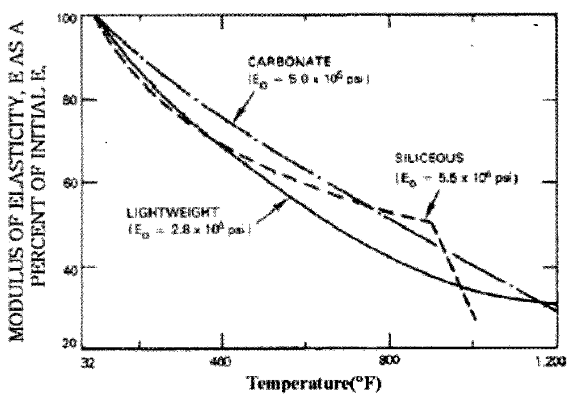

(b) Young's Modulus Ratio [8]

Fig. 3. Material Properties vs. Temperature

A smooth curve for strength degradation versus temperature, as estimated below (provided as a reference with temperature variation), is introduced into the finite element analysis model.

$$S_{temp\_rc} = e^{-(T/632)^{1.8}} \tag{7}$$

where T = Temperature in degrees Celsius. Further, based on the literature, the elastic modulus reduction is calculated by equation (8), as follows.

$$E_{temp\_rc} = \sqrt{S_{temp\_rc}} \tag{8}$$

S_{temp_rc} and E_{temp_rc} vs. temperature are shown in Fig. 4 (a). The thermal elongation is assumed nonlinear up to 700 °C, where it becomes constant [9].

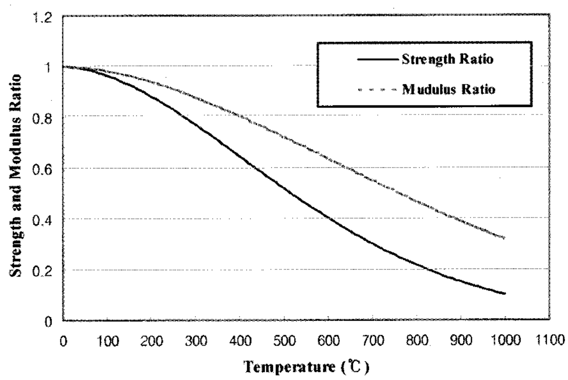

(a) Concrete

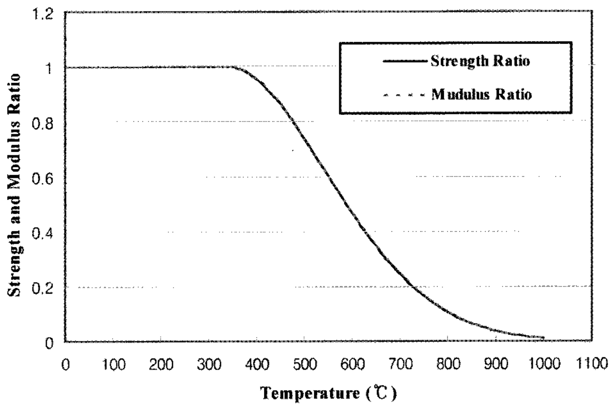

(b) Steel

Fig. 4. Material Properties Reduction vs. Temperature

In addition, the strength reduction of steel is considered in the analysis model, as depicited below based on previous research results [11] and shown in Fig. 4(b)

$$S_{temp\_rs} = e^{-[(T-340)/300]^{1.9}} \; for \;\; T > 340^{\circ}C$$
$$S_{temp\_rs} = 1.0 \;\; for \;\; T \leq 340^{\circ}C \qquad (9)$$

The thermal elongation is determined from the equations from the Eurocode 3 [12].

3. ANALYSIS UNDER TEST PRESSURE

3.1 Axisymmetric Finite Element Model

The axisymmetric finite element model consists only of the axisymmetric cylindrical vessel, a spherical dome and the concrete base slab. This model is intended to provide the general global behavior of the PCCV model considering an uplift of the base slab. This model consists of 809 eight-node axisymmetric solid elements, nonlinear soil spring elements, and 4,698 nodal points. The concrete structure is modeled with eight-node axisymmetric solid elements. The liner steel on the inside surface of the PCCV is made up of three-node shell elements. The liner elements, which are offset from the prestressed concrete elements, are connected to the concrete solid elements by rigid link elements. All rebars and tendons are assumed to remain rigidly bonded to the concrete. Vertical liner anchors are modeled as a beam of rectangular cross-section dimension. The tendon gallery is considered in the model. The floor liner plate is assumed to be rigidly connected to the eight-node concrete solid elements, since the effect of steel and concrete interaction during the flexural deformation of the slab is not significant with respect to the thick base slab of the PCCV. The bottom of the slab rests on a soil foundation, which is modeled by nonlinear soil springs with a tension cut-off.

3.2 Three-Dimensional Finite Element Model

The three-dimensional finite element model includes large penetrations, such as equipment hatches and air-locks, and two buttresses, which will cause deviation from an axisymmetric response and may decrease the capability of the PCCV. In order to simulate behavior near these regions more realistically, a more refined mesh is developed. In addition, a rigid interconnection between the shell element in the base slab and shell elements in the wall is introduced to properly simulate the shell/slab junction. The model consists of 1,720 four-node shell elements, nonlinear soil spring elements, and 1,425 nodal points.

The concrete structure is modeled with composite shell elements consisting of a thin inner layer of steel representing the liner and much thicker outer concrete multi-layers. As mentioned in the axisymmetric model, the tendons and rebars are similarly assumed to remain rigidly bonded to the concrete. The bottom of the slab rests on a soil foundation, which is modeled by the nonlinear soil spring with a tension cut-off.

3.3 Analysis Results

The pressure-radial displacement relationships by both FE analyses are compared in Figure 5. Analysis results using an axisymmetric FE model are a little larger than that those using a three-dimensional FE model are. The difference can be neglected, because the value is in an analysis uncertainty range.

Figures 6 through 8 shows the direct comparisons of the three-dimensional analysis and the measured results, which are the structural failure mode test (SFMT) results of 1:4 scale PCCV. The comparisons show that the analysis results are in good agreement with the test results. The recorded results of the liner from the SFMT were not meaningful to compare with the analysis results, since the liner plate was already torn partially during a limit state test.

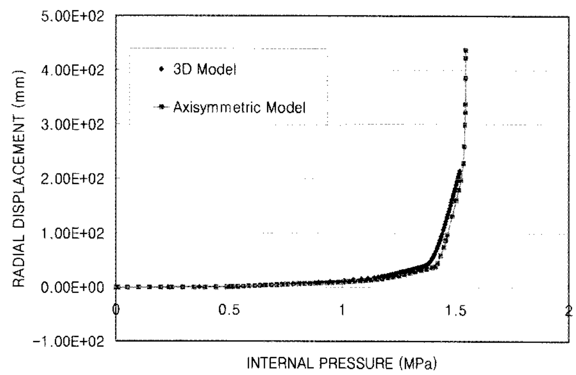

(a) Displacement

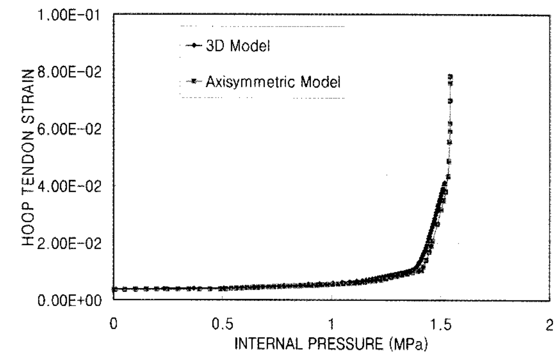

(b) Tendon strain

Fig. 5. Comparisons of 2D & 3D Analyses

4. ANALYSIS UNDER SEVERE ACCIDENT LOADING

4.1 Finite Element (FE) Analysis (2-D)

Because of the elastic support below the bottom slab, the effect of the weight of the structure had to be initially considered prior to internal pressurization and/or thermal loading. This is accomplished by specifying a mass proportional load for each material included in the 1:4

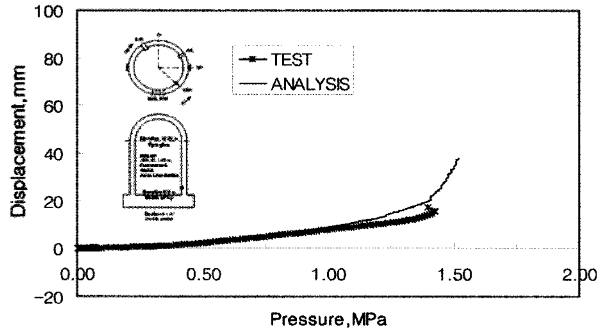

(a) Bottom of Cylindrical Wall

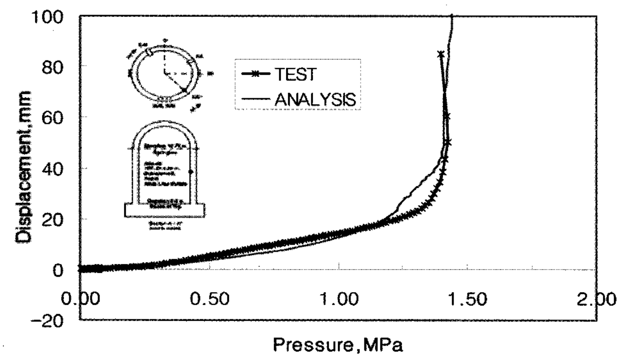

(b) Mid-height of Cylindrical Wall

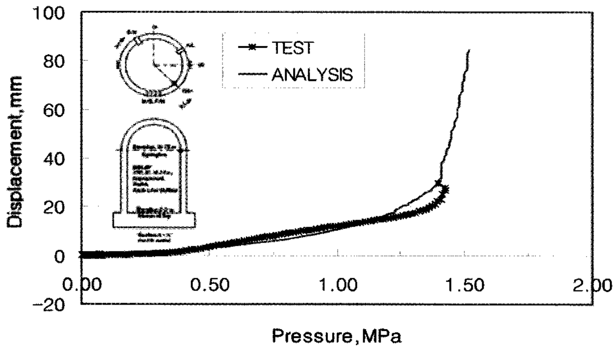

(c) Springline

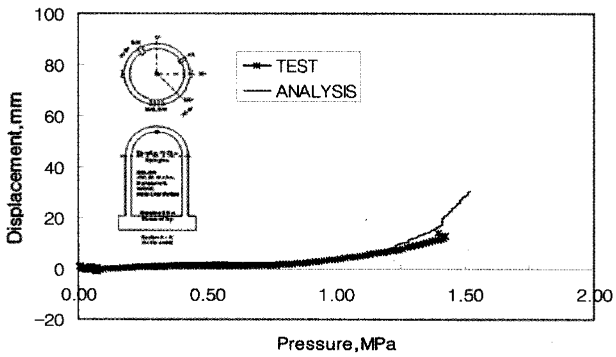

(d) Dome Apex

Fig. 6. Displacements of Test & Analysis Results

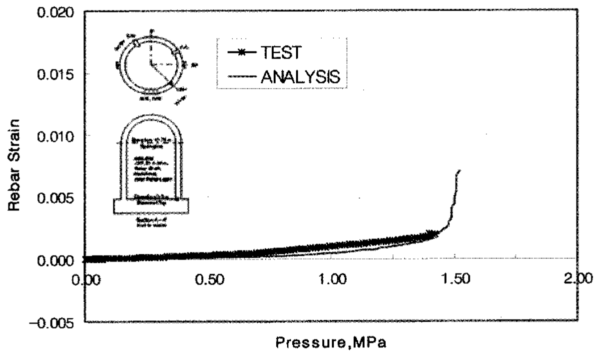

(a) Bottom of Cylindrical Wall

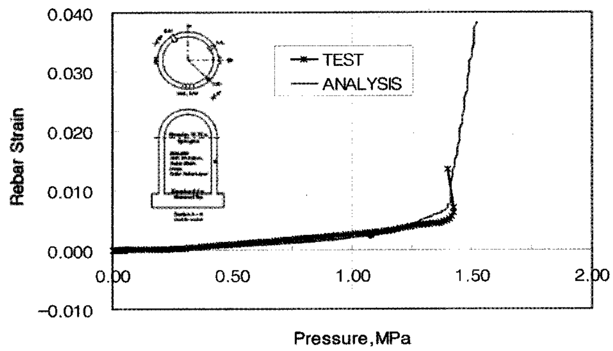

(b) Mid-height of Cylindrical Wall

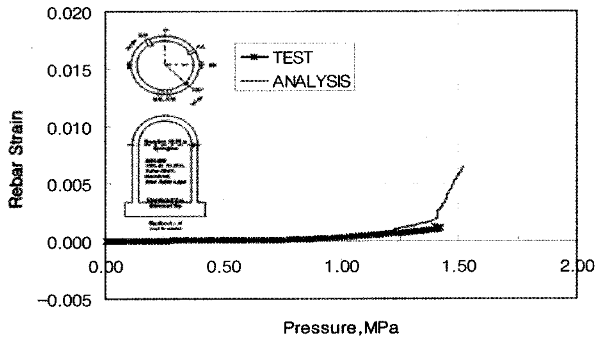

(c) Springline

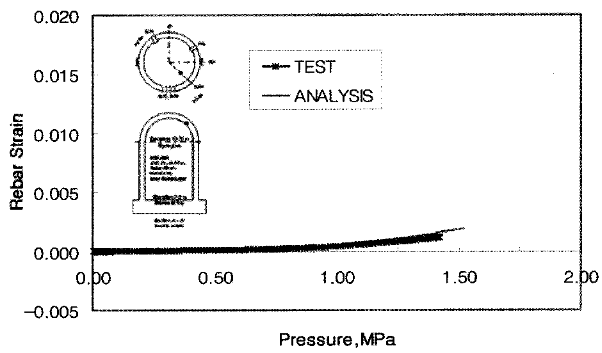

(d) Dome

Fig. 7. Rebar Strains of Test & Analysis Results

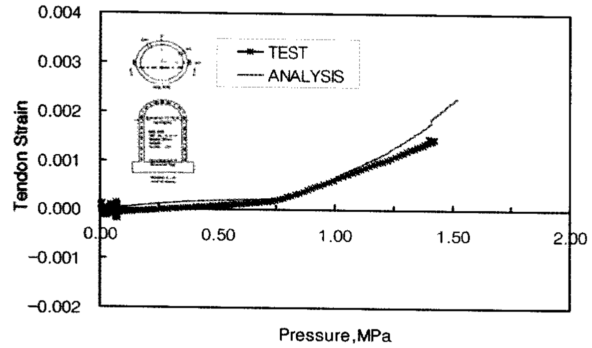

(a) Dome Apex (Meridional Tendon)

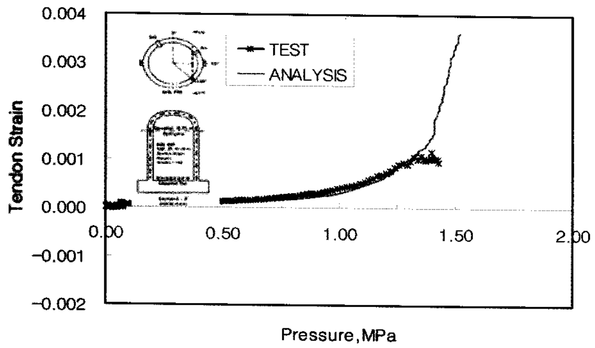

(b) Springline (Hairpin)

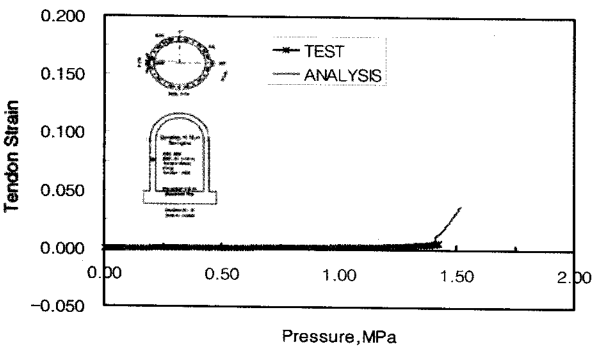

(c) Mid-height of Cylindrical Wall(Hoop Tendon)

Fig. 8. Tendon Strains of Test & Analysis Results

scale PCCV model prior to initiating the internal pressure and/or thermal loading.

The loading histories of internal pressure and thermal loading are shown in Figures 9 and 10. Figure 9 represents a saturated steam condition case, and Figure 10 shows a station blackout scenario with a hydrogen burn at about 4.5 hours into the accident event. Figure 10 shows the result of analyses performed by Sandia National Laboratories using MELCOR [13]. The heat distribution result through the wall thickness wall and base slab is achieved by heat transfer analyses. The thermal gradient specified at each thermal gradient section is identically applied to both halves of each thermal gradient section, as the thermal gradients of each neigh-boring thermal

Table 5. Load Cases

Load Case	Loading Combination
CASE 1	Dead Load + Effective Tendon Force + Saturated Steam Condition
CASE2	Dead Load + Effective Tendon Force + Station Blackout Scenario(SBO)

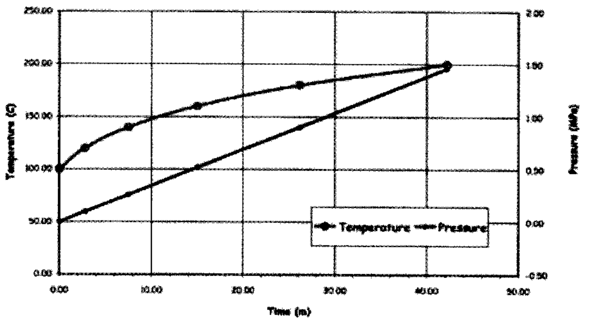

(a) Temperature and Pressure

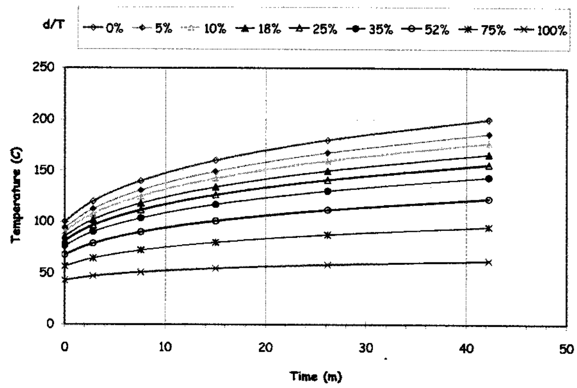

(b) Typical Temperature Distribution at Wall Section

Fig. 9. Loading Histories for Case 1

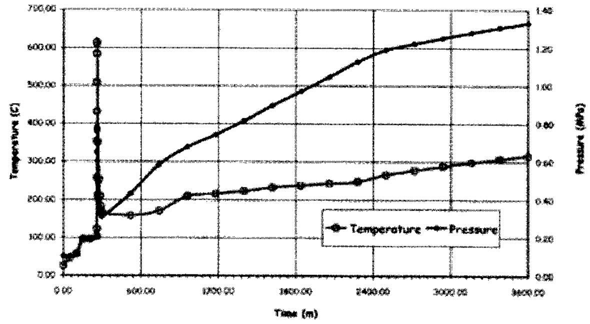

(a) Temperature and Pressure

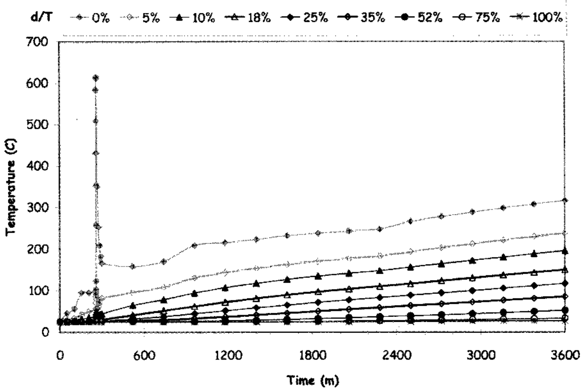

(b) Typical Temperature Distribution at Wall Section

Fig. 10. Loading Histories for Severe Accident Scenario

gradient section are not much different from those for each section. The temperature time history and pressure time history are applied at nodes of the finite element model. Table 5 is a summary of the loading cases.

The axi-symmetric finite element model, which is utilized to predict the overall response of the PCCV under internal pressurization and/or thermal loading is shown in Figure 11.

As shown in Figure 12, the radial displacements under pressure only correspond well with the numerical results and the measured displacements from SFMT. A combined mechanical-thermal analysis simulating a saturated steam condition (Case 1) shows that the temperature history, starting with 100°C, created a sudden initial increase in displacements, but the slopes expressing the pressure-displacement relationship with increasing temperature and pressure appeared very similar to the trend for the pressure only case.

The analysis results for Case 2 show that the displacements due to the sudden increase in temperature and pressure for a very short time period did not fully recover when returned to the starting temperature and pressure. This result can be interpreted as residual deformation from damage to the liner plate and/or concrete portion due to instantaneous high temperature and pressure loading. Unfortunately, the analysis for Case 2 was stopped at 1.1974 MPa due to divergence, and the behaviors could not be investigated beyond 1.1974 MPa. The ultimate capacity may drop rapidly with a sudden increase in deformation, which in turn will induce divergence (see Figures 12 through 14).

Figure 13 shows that the strains in the reinforcements under pressure only compare well with the numerical results and the measured displacements from SFMT. A combined mechanical-thermal analysis simulating a saturated steam condition (Case 1) shows that the thermal loading history starting with 100°C created an abrupt initial increase in strains similar to the displacements, but the slopes expressing the pressure-displacement relationships with increasing temperature and pressure appeared closer to the trend for pressure only.

The analysis results for Case 2 shows that the rebar strains due to the sudden increase of temperature and pressure for short durations do not fully return to the strains at initial pressure and temperature. This result can be interpreted as residual deformation from damage to the liner plate and/ or concrete portion due to instantaneous high temperature and pressure loading.

Maximum compressive stresses in the liner versus the corresponding pressure loadings are shown in Figure 14. Case 2 shows that the stresses in the liner were under compressive behavior at pressures between 0.2 MPa and 0.78 MPa and temperatures between 100°C and 615°C for short periods of around 260 through 300 minutes. Stresses of Case 2 are beyond the buckling stress of 122 MPa, considering the horizontal spacing of liner anchor.

The pressure levels corresponding to loading cases are summarized in Table 6. In case 1, the pressure levels to reach initial concrete crack, rebar yielding, and liner rupture are slightly lower than those in the case of pressure only but are negligible in view of security of safety. On the other hand, in Case 2, the pressure levels to reach initial concrete crack, yielding of liner steel and rebar, and liner rupture are considerably lower than when subjected to pressure only.

Table 6. Comparisons of Pressure Levels (MPa)

Item	Pre. Only	Case 1	Case 2
Initial concrete crack	0.60	0.60	0.60
Yielding of liner steel	0.75	1.03	0.46
First yield of hoop rebar	1.16	0.88	0.78
Liner 1% strain	1.03	1.20	0.46
Tendon yielding	1.43	1.41	-
Tendon 3% strain	1.51	1.47	-

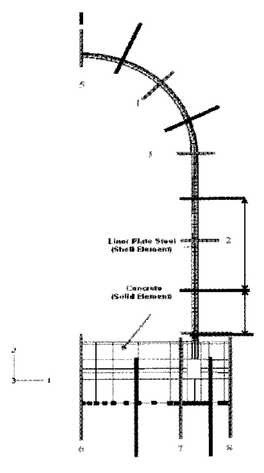

Fig. 11. Loading History for Severe Accident Scenario

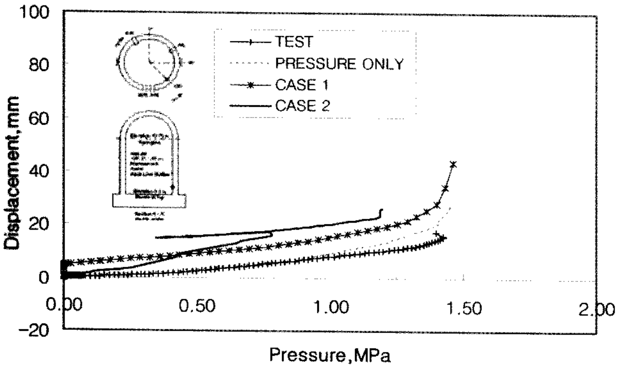

(a) Bottom of Cylindrical Wall

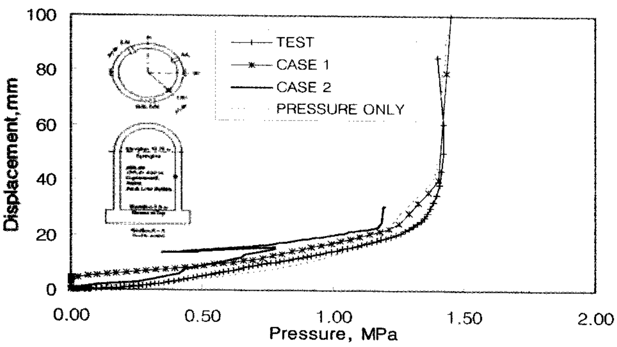

(b) Mid-height of Cylindrical Wall

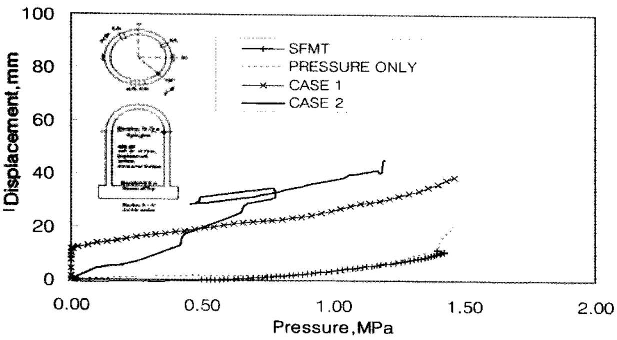

(c) Springline

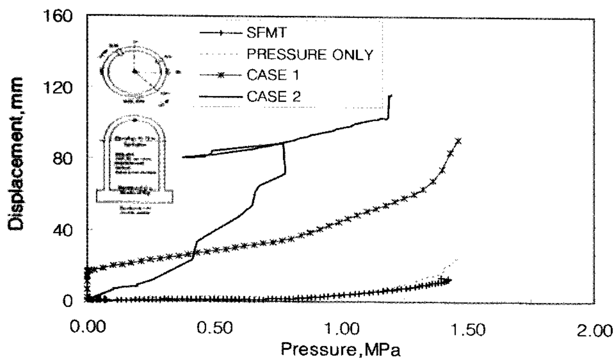

(d) Dome Apex

Fig. 12. Comparison Results of Displacements

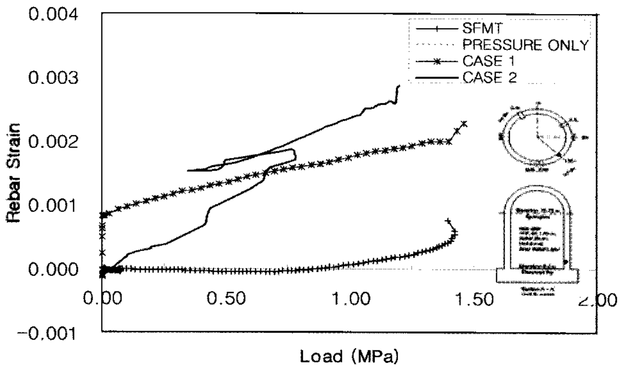

(a) Bottom of Cylindrical Wall

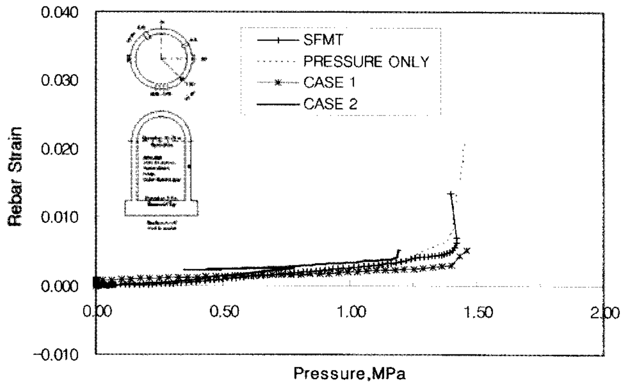

(b) Mid-height of Cylindrical Wall

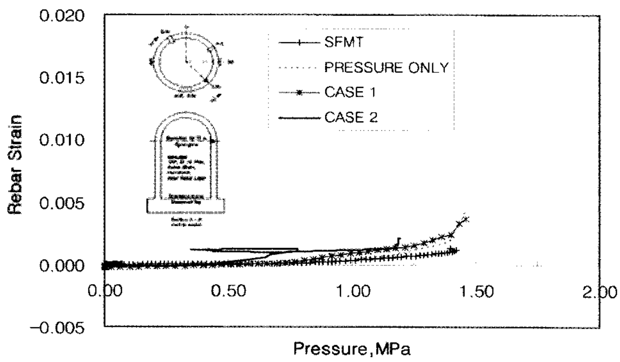

(c) Sprlingline

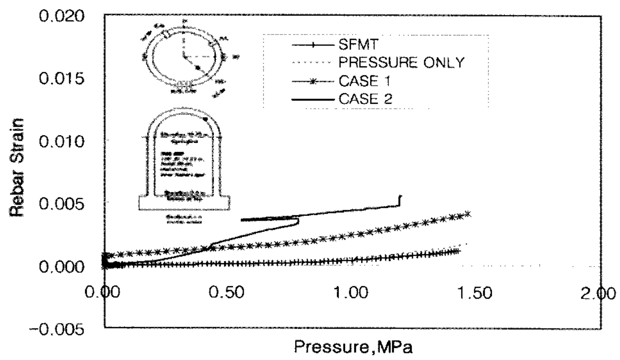

(d) Dome

Fig. 13. Comparison Results of Rebar Strains

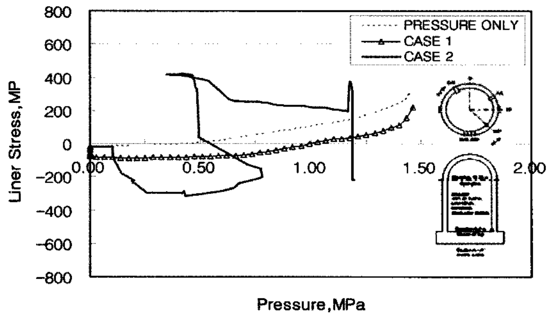

(a) Base of Cylindrical Wall

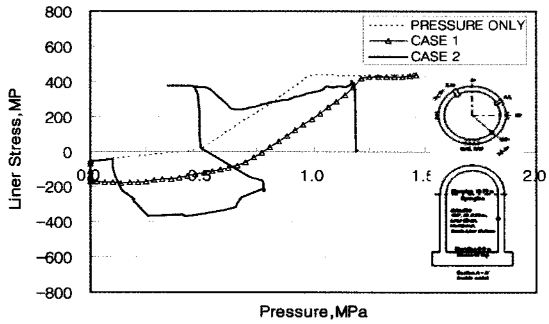

(b) Mid-height of Cylindrical Wall

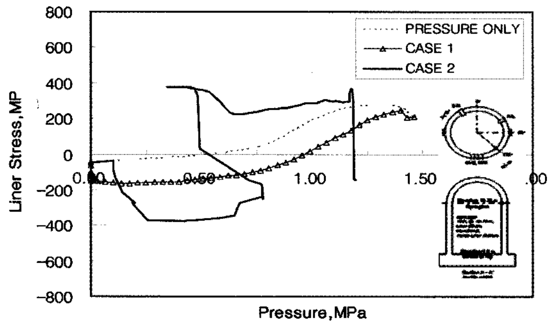

(c) Springline

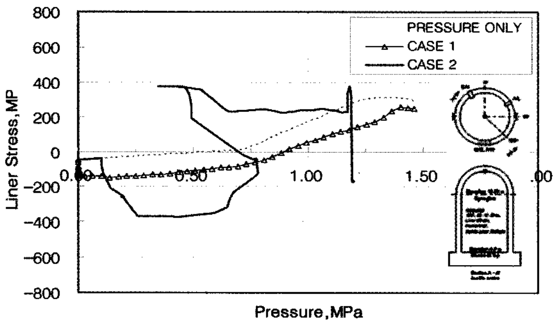

(d) Dome Apex

Fig. 14. Comparison Results of Displacements

5. CONCLUSIONS

1) The nonlinear behavior of PCCV under internal pressure loading is slightly influenced by the non-symmetrical characteristics of the structure.
2) The constitutive models of the material introduced here are confirmed to be able to avoid numerical instability up to the ultimate pressure capacity of PCCV.
3) Analyses of PCCV under severe accident loading, especially with high temperature histories, were performed in this study.
4) For a design basis accident that contains temperature histories under 200 °C, the analyses results are similar to those of a pressure only case; therefore, the effects of temperature on the ultimate capacity of PCCV are negligible.
5) For a severe accident case that contains temperature histories over 300 °C, the structural behavior of PCCV is largely affected by temperature; therefore, the effects of temperature should be considered in safety evaluations of PCCV.

REFERENCES

[1] Hessheimer, M.F., Klamerus, E.W., Lambert, L.D. and Rightley, G.S., *Overpressurization Test of a 1:4-Scale Prestressed Concrete Containment Vessel Model*, NUREG/CR-6810, SAND2003-0840P, Sandia National Laboratories, Albuquerque, March 2003.
[2] Smith, S., 'On Fundamental Aspects of Concrete Behavior', MSc Thesis, University of Colorado, 1987.
[3] Ph Menetrey and K. J. Willam, 'Triaxial Failure Criter-ion for Concrete and Its Generation', ACI Structural journal, Vol. 92, No. 3, 1995, p.311-318.
[4] Wai-Fah Chen, 'Constitutive Equations for Engineering Materials', (Elsevier, 1994).
[5] Hajime Okamura and Kohichi Maekawa, 'Nonlinear Analysis and Constitutive Models of Reinforced Concrete', (Kibodang, 1990).
[6] Hsu, T.T.C., *Unified Theory of Reinforced Concrete*, CRC Press 1993, 205-218 pp.
[7] Khoury, G.A., "Compressive Strength of Concrete at High Temperatures: a Reassessment," Magazine of Concrete Research, 44, No. 161, Dec., pp. 291-309, 1992.
[8] Abrams, M. S., "Compressive Strength of Concrete at Temperatures to 1600°F," Temperature and Concrete, ACI SP-25, American Concrete Institute, pp. 33-58, 1971.
[9] EC2, 'Eurocode 2: Design of Concrete Struc-tures. ENV 1992-1-2: General Rules-Structural Fire Design', European Committee for Standardisation, 1993.
[10] Klinski, M., 'Degradation and Plastic Deformation of Concrete', IFTR Report 38, PhD thesis, Polish Academy of Science, 1985.
[11] Holmes, M., Anchor, R.D., Cook, M.D. and Crook, R.N., "The Effects of Elevated Temperatures on the Strength Properties of Reinforcing and Prestressing Steels", The Structural Engineer, Vol. 60B, No. 1, March 1982.
[12] EC3, 'Eurocode 3: Design of Steel Structures. ENV 1993-1-2: General Rules-Structural Fire Design', European Committee for Standardisation, 1995.
[13] MELCOR Computer Code Manuals, NUREG/CR-6119, SAND2000-2417, Sandia National Laboratories, Albuquerque, NM, December, 2000.